

## Implications of the recent $^{59}\text{Co}(n,p)^{59}\text{Fe}$ experiment for stellar electron capture rates

Maurice B. Aufderheide, Stewart D. Bloom, David A. Resler, and Grant J. Mathews

*Physics Department, Lawrence Livermore National Laboratory, Livermore, California 94550*

(Received 28 May 1992)

We study results from the recent measurement of the  $0^+ \ ^{59}\text{Co}(n,p)^{59}\text{Fe}$  cross section in order to compute the stellar electron capture rate of  $^{59}\text{Co}$ . This nucleus is the second most important electron capture nucleus in the core of a type II supernova progenitor just before core collapse. It is also the first nucleus which has a large effect on the stellar neutronization rate for which Gamow-Teller strength has been measured. The Gamow-Teller resonance has been observed experimentally at a higher energy above the daughter ground state than one would expect from independent particle shell model arguments, but large-basis shell model calculations employing configuration mixing are more successful in predicting the location of the strength. Because of the high energy of the Gamow-Teller resonance, the stellar electron capture rate and associated neutronization is much less than previous estimates had indicated. Similar trends are seen for  $^{60}\text{Co}$ , the most important electron capture nucleus for supernova progenitors just before core collapse.

PACS number(s): 97.10.Cv, 25.40.Fq, 97.60.Bw, 21.60.Cs

### I. INTRODUCTION

Gamow-Teller (GT) strength is an important component of stellar electron capture reactions in the cores of type II supernova progenitors [1]. Because electrons are degenerate in this environment, they are able to induce transitions to states with large GT strength several MeV above the daughter ground state. Fuller, Fowler, and Newman (FFN) [2–5] were the first to include this physics in a large tabulation of weak interaction rates. Their work showed that these rates are important for an accurate description of the formation of the iron core [6].

Charge-exchange experiments are at present the only probe of GT strength in nuclei over large ranges of excitation energy. There is, however, a current controversy about how accurately charge-exchange reactions can extract GT strength. A recent experiment by Garcia *et al.* [7] has called into question the accuracy of charge-exchange reactions as a measure of GT strength. They measured the  $\beta^+$  decay of  $^{37}\text{Ca}$ , the isospin mirror of  $^{37}\text{Cl}$ , over roughly 8 MeV of energy and compared it with the results of a  $^{37}\text{Cl}(p,n)^{37}\text{Ar}$  experiment [8]. It was claimed that on the order of 50% more strength was seen by the  $\beta^+$  decay experiment. However, most of this difference is seen in the region of the isobaric analog state and can be explained by the difficulty in distinguishing Fermi strength from Gamow-Teller strength [9] in the  $(p,n)$  experiment. The  $(n,p)$  reaction does not have this problem because there is no analog state accessible in this direction. The situation is still unresolved [10], but here we assume that charge-exchange experiments do accurately determine GT strength.

In estimating the location of GT strength, FFN built a simple shell model picture for each nucleus considered, without configuration mixing. This model has been called the independent single particle shell model (ISPSM) [11]. No relevant  $(n,p)$  experiments had been done at the time of FFN's work. Aufderheide [12] used the result of a  $^{54}\text{Fe}(n,p)^{54}\text{Mn}$  experiment [13] to test the

FFN approach. His estimates used the ISPSM of FFN, but started with the strength function measured by  $^{54}\text{Fe}(n,p)^{54}\text{Mn}$ . He found agreement with FFN to within a factor of 2 for  $^{54}\text{Fe}$ , but found larger differences from the FFN rates for  $^{53}\text{Mn}$ ,  $^{55}\text{Fe}$ ,  $^{59}\text{Co}$ , and  $^{60}\text{Co}$ . These differences could have a large effect on the evolution of the electron fraction ( $Y_e$ ) in stellar evolution calculations.

Recently, the distributions of GT strength for  $^{59}\text{Co}_{\text{g.s.}} \rightarrow ^{59}\text{Fe}$  has been measured at TRIUMF using the  $^{59}\text{Co}(n,p)^{59}\text{Fe}$  reaction at 200 MeV [14,15]. Just before a presupernova core begins its final collapse, the central density is of the order of  $10^9 \text{ g cm}^{-3}$ ,  $T_9$  (the temperature in  $10^9 \text{ K}$ ) is near 4.5, and  $Y_e$  is near 0.43. In these conditions  $^{59}\text{Co}$  is the second most important electron capture nucleus after  $^{60}\text{Co}$  (in terms of the neutronization it engenders). Thus this is the first case where a charge-exchange experiment has measured Gamow-Teller strength for a nucleus which plays an important role in the neutronization of the presupernova core. Extrapolation [12] from  $^{54}\text{Fe}$  is no longer necessary. In this paper we will use the strength function extracted from this experiment to compute the stellar electron capture rate. In the next section, we discuss the GT strength function and compare it with previous estimates. We also examine transitions to low lying states in  $^{59}\text{Fe}$  which are seen in the  $(n,p)$  data. In the third section, shell model calculations are performed for comparison with the measured strength function and to obtain GT strength functions for excited states. In the fourth section, we compute stellar electron capture rates for  $^{59}\text{Co}$  combining all experimentally known information and shell model results for excited states. In the fifth section, we use shell model calculations, informed by the experimental results, to compute electron capture rates on  $^{60}\text{Co}$ .

### II. THE $(n,p)$ EXPERIMENT

Figure 1 shows the GT strength for  $^{59}\text{Co}(n,p)^{59}\text{Fe}$  as measured [14,15] by TRIUMF experiment E629 as a

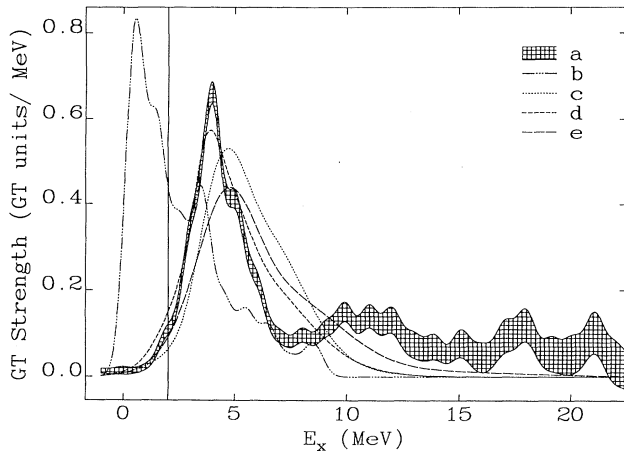


FIG. 1. Measured [14,15] GT strength (curve *a*) compared with an ISPSM estimate [12] (curve *b*) and the shell model results (curves *c*–*e*). The crosshatched region for curve *a* shows the present range of experimental uncertainty. The vertical line shows when FFN placed the centroid of the resonance. Curves *c*, *d*, and *e* are the strength functions from the small, small modified, and large shell model spaces, respectively. The shell model strength functions are given the widths assigned them by the Lanczos process after ten iterations for each allowed daughter  $J^\pi$ , added in quadrature with the experimental resolution of 1 MeV (full width at half maximum). The shell model results have been quenched by factors of 0.291, 0.342, and 0.358 for the small, small modified, and large shell model spaces, respectively (see Table IV). The experiment and ISPSM estimates have been plotted with the experimental resolutions of 1 MeV.

function of daughter excitation energy. The strength is peaked near  $E_x = 4$  MeV in  $^{59}\text{Fe}$ . It is surprising that the strength is so high above the ground state of  $^{59}\text{Fe}$ . In the  $^{54}\text{Fe}(n,p)^{54}\text{Mn}$  reaction, the GT peak is much closer to the daughter ground state ( $\sim 1.5$  MeV). The independent single particle shell model would predict that the strength is even closer to the daughter ground state in  $^{59}\text{Co}$  than in  $^{54}\text{Fe}$ . This is a consequence of the additional filling of neutron orbitals in  $^{59}\text{Co}$ .  $^{59}\text{Fe}$  has a filled  $2p_{3/2}$  orbital, whereas  $^{54}\text{Mn}$  does not. An ISPSM estimate for the strength function [12], made by extrapolation from  $^{54}\text{Fe}$ , is also shown in Fig. 1. Clearly, this extrapolation is not in agreement with the measured strength. The original methods of FFN would have placed the centroid of the resonance at 2 MeV, still too close to the daughter ground state.

The total GT strength is also surprising. The  $^{54}\text{Fe}$  experiment measured  $B(\text{GT})_+ = 3.09 \pm 0.57$  below 10 MeV in units where the GT sum rule [16] gives  $B(\text{GT})_- - B(\text{GT})_+ = 3(N - Z)$ . From the  $^{54}\text{Fe}$  experiment, it can be estimated that for  $^{59}\text{Co}$ ,  $B(\text{GT})_+ = \frac{7}{6}(3.09) = 3.6$ , where the  $\frac{7}{6}$  factor corrects for the extra proton which can be converted into a neutron in  $^{59}\text{Co}$ . The experiment has measured  $B(\text{GT})_+ = 2.39 \pm 0.07$  below 12.5 MeV. Again, the naive expectations

are not satisfied. This unexpected weakness in strength and the high energy of the GT strength suggest that excitations out of the filled  $2p_{3/2}$  neutron orbital into the  $1f_{5/2}$  orbital block the GT transitions and push them to higher energies. This intuition is borne out by shell model calculations with configuration mixing, as will be seen.

Relatively little GT strength is seen below 4 MeV in  $^{59}\text{Fe}$ . The first two bins of GT strength range from  $-0.5$  to  $0.5$  MeV and from  $0.5$  to  $1.5$  MeV. The strength in these bins is  $1.31(-2) \pm 0.91(-2)$  and  $1.70(-2) \pm 0.65(-2)$ , respectively. An examination of the low energy spectrum of  $^{59}\text{Fe}$  explains this weakness.  $^{59}\text{Co}$  has a  $J^\pi$  of  $\frac{7}{2}^-$ , and allowed GT transitions can thus go to states with  $J^\pi = \frac{5}{2}^-$ ,  $\frac{7}{2}^-$ , and  $\frac{9}{2}^-$ . Below 2 MeV, only two states can have allowed GT transitions: a  $\frac{5}{2}^-$  state at 0.472 MeV and a  $\frac{7}{2}^-$  state at 1.023 MeV. The former state straddles the two lowest bins of GT strength. This means that the strength in this state is fairly evenly divided between the two bins. Thus we assume that  $1.31(-2)$  units of GT strength in each bin resides in the 0.472 MeV state:  $B(\text{GT})_+ = 2.62(-2) \pm 1.04(-2)$ . The rest of the strength in the second bin is assumed to reside in the 1.023 MeV state:  $B(\text{GT})_+ = 3.90(-3) \pm 1.49(-3)$ . Using the relation [17]

$$\log_{10} f t_{ij} = \log_{10} \frac{K}{|g_A/g_V|^2} - \log_{10} B_{ij}(\text{GT}), \quad (1)$$

where  $B_{ij}(\text{GT})$  is the GT strength from the  $i$ th parent state to the  $j$ th daughter state,  $K = 6170$  sec, and  $|g_A/g_V|^2$  has the observed value [18] of  $(1.262)^2$ ; the  $\log f t$  for the transitions from the  $^{59}\text{Co}$  ground state to the  $^{59}\text{Fe}$   $\frac{5}{2}^-$  state at 0.472 MeV and the  $^{59}\text{Fe}$   $\frac{7}{2}^-$  state at 1.023 MeV are  $5.17 \mp_{0.22}^{0.14}$  and  $6.00 \mp_{0.21}^{0.14}$ , respectively, which are reasonable values.

### III. USING THE SHELL MODEL

The nuclei which are of interest in this paper,  $^{59}\text{Co}$  and  $^{60}\text{Co}$ , are nuclei which contain 19 and 20, respectively, active nucleons in the  $fp$  shell. Shell model studies of  $fp$  shell nuclei are still in their infancy, mainly because of the size of the model spaces involved. Performing  $0\hbar\omega$  full  $fp$  shell model calculations for these nuclei would require computers which could handle model spaces with dimensions of  $6.75 \times 10^8$  ( $^{59}\text{Co}$ ) and  $4.23 \times 10^8$  ( $^{60}\text{Co}$ ). In this paper we are thus limited to what is (roughly) the state of the art: calculations with dimensions of less than approximately  $10^5$ . Such limitations force us to truncate the  $fp$  shell model space. As will be discussed below, we have followed a standard truncation of limiting the number of nucleons which are free to move within the  $(2p_{3/2}, 2p_{1/2}, 1f_{5/2})$  manifold. However, this truncation is performed in such a way that the GT sum rule is not compromised. The sum rule is preserved by calculating daughter properties at one nucleon more of excitation than for the parent space.

When one considers the level of truncation which we employ, it is surprising that any features of the GT strength functions are reliably reproduced. However, the collective nature of GT resonances is robust enough that

it is adequately represented in even the small model spaces considered here.

Obviously, what is seen in the experiment is not a truncated  $fp$  shell nucleus or even a full  $fp$  shell nucleus, but rather a nucleus with all orders of excitations within and out of the  $fp$  shell. The differences between our calculations and what is seen experimentally is a measure of what the physics we have excluded contributes to the strength functions. One such contribution is the total amount of strength observed. As will be seen below, increasing the number of nucleons which are free to move in the  $(2p_{3/2}, 2p_{1/2}, 1f_{5/2})$  manifold tends to reduce the total amount of strength by blocking GT transitions. Thus, if it were possible to perform a full  $fp$  shell model calculation for these nuclei, it is likely that we would need to quench our calculation less severely than is required for the truncated results described below. Including multi- $\hbar\omega$  excitations out of (and into) the  $fp$  shell would further complicate the situation. Neutron excitations out of the  $fp$  shell could increase the amount of GT strength, by opening up more GT transitions. However, neutron excitations into the  $fp$  shell from filled shells could vitiate this effect. Also, proton excitations out of the  $fp$  shell could weaken the amount of strength by making less protons available for GT transitions. We can make no definitive statements about these effects because they are inaccessible to us. In our limited calculations, we assume that the quenching seen in the ground state of  $^{59}\text{Co}$  is typical for its excited states and also for neighboring nuclei.

The FPVH interaction [19,20] has been fairly successful at modeling the GT strength measured in  $(p,n)$  reactions [21]. This interaction was designed for modeling nuclei in the iron region with a defined model space. For  $A \sim 54$ , the model space is

$$(1f_{7/2})^n + (1f_{7/2})^{n-1}(2p_{3/2}, 2p_{1/2}, 1f_{5/2})^1,$$

where  $n$  is the number of nucleons in the  $fp$  shell. For  $A > 60$ , the model space is  $(1f_{7/2})^{16}(2p_{3/2}, 2p_{1/2}, 1f_{5/2})^k$ , where  $n = 16 + k$  and the  $^{56}\text{Ni}$  core is closed. Thus only the  $k$  nucleons above this core are free to move.

$^{59}\text{Co}$  is an intermediate case. It is similar to the  $A > 60$  nuclei, except that it is one proton short of the  $^{56}\text{Ni}$  core. In this study we consider two model spaces for  $^{59}\text{Co}$ . In the first we treat the  $^{55}\text{Co}$  core as "closed" and allow no excitations from it. The four neutrons above this core are free to couple within the  $(2p_{3/2}, 2p_{1/2}, 1f_{5/2})$  space. The second model space includes the previous smaller space and, in addition, allows one  $1f_{7/2}$  nucleon to be excited up into the  $(2p_{3/2}, 2p_{1/2}, 1f_{5/2})$  space. The first excited state of  $^{59}\text{Co}$ , the  $\frac{3}{2}^-$  state at 1.099 MeV, does not appear in the former model space because no excitations from

TABLE II. Single particle energies. All energies are given in MeV.

Orbital	FPVH	Modified FPVH
$1f_{5/2}$	-0.2630	-1.2630
$2p_{1/2}$	-2.4740	-2.4740
$2p_{3/2}$	-5.3530	-5.3530
$1f_{7/2}$	-7.1630	-7.1630

$1f_{7/2}$  to  $2p_{3/2}$  have been allowed. In order to satisfy the sum rule, higher order excitations must be included in the computation of the daughter nucleus. The  $^{59}\text{Fe}$  model spaces corresponding to these parent model spaces are given in Table I. Dimensions of the spaces are also given.

Figure 1 also shows the strength functions computed for these model spaces, in comparison with the ISPSM estimate and the  $(n,p)$  measurement. The CRUNCHER shell model code [22] was used to generate these strength functions. The Lanczos method has been used to compute the first nine moments of the strength function for each allowed daughter  $J^\pi$  value. In this way enough information has been obtained to calculate rates, without performing a full diagonalization of the daughter space.

These shell model calculations place the GT strength much higher above the ground state of  $^{59}\text{Fe}$  than did the ISPSM estimate. The difference is due to configuration mixing and residual interaction effects which a full shell model calculation can include. It can be seen that the shell model calculations are much closer to the actual strength than the ISPSM estimate was. The large model space tends to spread the strength higher and over a larger region in daughter excitation energy, as a result of the added configuration mixing. The centroid of the strength in the small space is 5.58 MeV, while in the large space the centroid is 6.22 MeV.

It is possible to improve the agreement of the shell model calculation with the experiment by shifting the  $1f_{5/2}$  orbital to lower energy. This has been done for the small model space. It was found that a 1 MeV shift downward is required to fit the main resonance. The single particle energies used in the two calculations are given in Table II. Unfortunately, such a shift adversely affects the low energy spectrum of the parent nucleus. This is not surprising because the interaction was developed for a particular set of single particle energies. This effect is seen in Table III, where the  $^{59}\text{Co}$  spectrum is shown for all three shell model calculations. The case with the shifted  $1f_{5/2}$  orbital has poorer agreement with the actual spectrum than does the small model space calculation. The large model space also has poorer agree-

TABLE I. Dimensions for  $^{59}\text{Co}$  calculations.

$^{59}\text{Co}$		$^{59}\text{Fe}$	
Model space	Dim.	Model space	Dim.
$(1f_{7/2})^{15}(2p_{3/2}, 2p_{1/2}, 1f_{5/2})^4$	447	$(1f_{7/2})^{14}(2p_{3/2}, 2p_{1/2}, 1f_{5/2})^5$	2170
$+(1f_{7/2})^{14}(2p_{3/2}, 2p_{1/2}, 1f_{5/2})^5$	20 858	$+(1f_{7/2})^{13}(2p_{3/2}, 2p_{1/2}, 1f_{5/2})^6$	66 425

TABLE III.  $^{59}\text{Co}$  spectrum. All energies are in MeV.

$J^\pi$	Experimental	Small	Small modified	Large
$\frac{7}{2}^-$	0.000	0.000	0.000	0.000
$\frac{3}{2}^-$	1.099	a	a	1.179
$\frac{5}{2}^-$	1.190	1.298	1.387	1.119
$\frac{3}{2}^-$	1.291	1.501	1.614	a
$\frac{1}{2}^-$	1.435	3.524	3.544	2.055
$\frac{11}{2}^-$	1.459	1.463	1.444	1.211
$\frac{5}{2}^-$	1.482	1.709	1.844	1.372
$\frac{7}{2}^-$	1.745	1.824	2.007	1.458
$\frac{7}{2}^-$	2.063	1.933	2.165	1.622

<sup>a</sup>States which do not appear in a particular calculation.

does the small model case. None of these models produce two  $\frac{3}{2}^-$  states, and it is difficult to identify which of these states corresponds most closely to the shell model states.

#### IV. STELLAR ELECTRON CAPTURE RATE

The iron core of a type II supernova progenitor is an environment with temperatures of roughly  $3 \times 10^9$  K and higher. In such conditions, nuclei are thermally excited and the GT strength function from each of the excited parent states must be included in the total rate. This rate can be written as

$$\lambda_{Z,A}(\rho, T, Y_e) = \ln 2 \sum_i \frac{(2J_i + 1) \exp[-E_i/k_B T]}{G(Z, A, T)} \times \sum_j \frac{\phi(\rho, T, Y_e, Q_{ij})}{ft_{ij}}, \quad (2)$$

where  $\rho$ ,  $T$ , and  $Y_e$  are the density, temperature, and electron fraction, respectively,  $i$  denotes parent states,  $j$  denotes daughter states,  $J_i$  and  $E_i$  are the spin and excitation energy of the  $i$ th parent state,  $G$  is the nuclear partition function,  $\phi$  is the standard electron capture phase space integral as defined in Aufderheide [12], and  $Q_{ij}$  is the nuclear energy difference between states  $i$  and  $j$ . The  $^{59}\text{Co}$  experiment gives  $B_{0j}(\text{GT})_+$ . Various shell model calculations will be used to compute the strength function for excited states of  $^{59}\text{Co}$  and fold them into Eq. (2).

Figure 2 shows the strength functions computed for each of the shell model excited states. The functions are plotted in the order in which the parent states appear in each shell model calculation. In the FFN rate estimates, the centroid of the strength function of each excited state was assumed to move by the same amount as the parent state, relative to the parent ground state. This has been called [12] the Brink assumption [23] and is tested in Table IV. As can be seen, the Brink assumption is satisfied to within roughly 100–200 keV. The shifted case obeys this assumption less well: only to within 250

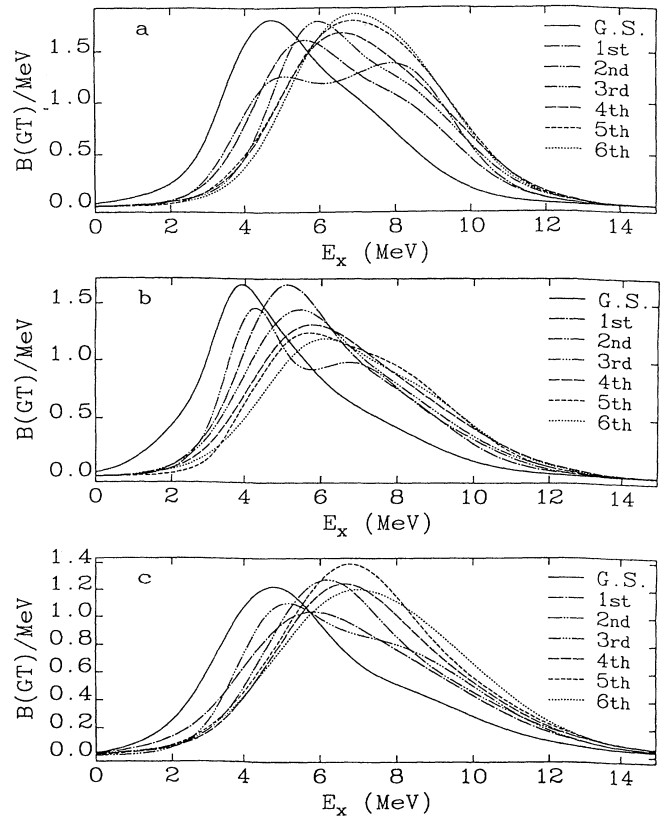


FIG. 2. GT strength functions for the ground states of  $^{59}\text{Co}$ . The strength functions from the parent states listed in Table III are listed in the order in which each parent state appears in a particular shell model calculation. The shell model strength functions are given the widths assigned them by the Lanczos process after ten iterations for each allowed daughter  $J^\pi$ , added in quadrature with the experimental resolution of 1 MeV (full width at half maximum). None of the strength functions have been quenched. (a), (b), and (c) correspond to the small, small modified, and the large model spaces, respectively.

TABLE IV. GT strengths and centroids for  $^{59}\text{Co}$ . All energies are given in MeV. The centroid of the strength function corresponding to the  $i$ th  $^{59}\text{Co}$  excited state is  $\bar{E}_i$ .  $\bar{E}_0$  is the centroid of the strength function from the ground state of  $^{59}\text{Co}$ .  $Q$  is the quenching factor to be used for each calculation.

Small space			Small modified space			Large space		
$E_i$	$\bar{E}_i - \bar{E}_0$	$B(\text{GT})$	$E_i$	$\bar{E}_i - \bar{E}_0$	$B(\text{GT})$	$E_i$	$\bar{E}_i - \bar{E}_0$	$B(\text{GT})$
0.000	0.000	8.22	0.000	0.000	6.98	0.000	0.000	6.68
1.298	1.100	8.10	1.387	1.150	7.45	1.119	0.950	6.74
1.463	1.310	8.40	1.444	1.200	6.84	1.179	1.260	7.13
1.501	1.470	8.60	1.614	1.424	7.23	1.211	1.120	6.91
1.709	1.670	8.70	1.844	1.739	7.06	1.372	1.490	7.24
1.824	1.710	9.34	2.007	1.880	6.74	1.458	1.470	7.92
1.933	1.790	9.17	2.165	1.970	6.45	1.622	1.650	7.65
$Q = \frac{2.39}{8.22} = 0.291$			$Q = \frac{2.39}{6.98} = 0.342$			$Q = \frac{2.39}{6.68} = 0.358$		

keV. The small model space and the large model space show the same trend of slightly increasing strength with increasing parent excitation energy. The large space shows roughly 20% less strength than the small space does. This is another confirmation that more excitations tend to “block” the GT strength. The results from using the small modified space show a diminution in strength similar to what was seen in the large model space. By bringing the  $1f_{5/2}$  orbital closer to the  $2p_{3/2}$  orbital, one-particle–one-hole (1p-1h) excitations become easier, thus blocking GT transitions more effectively. The small modified space produces strengths which tend to diminish with increasing excitation energy.

As can be seen in Table IV, the total GT strength measured in the experiment was much less than the amount predicted by any of these shell models. This is the phenomenon of quenching [24] of the GT strength. When computing the stellar electron capture rates from the shell model strength functions, each strength function has been quenched by the factor  $Q = 2.39/B_0(\text{GT})$ , where  $B_0(\text{GT})$  is the total calculated strength from the parent ground state to the daughter for each shell model.

It can be seen in Table III that for each shell model calculation several of the parent states are in the wrong place. In the rate calculation, these parent states have been shifted to their correct energies and their corresponding strength functions have been shifted in the same manner. This is consistent with the Brink assumption, as was justified in Table IV. Table III also shows that, in some cases, there was no parent state available for computing a strength function. In these cases the nearest state with similar  $J^\pi$  was used as the parent and the resulting strength function was shifted so as to satisfy the Brink assumption.

The FFN rates were composed of two main components: resonant transitions at relatively high energy and weak transitions between relatively low-lying states in the parent and daughter nuclei. For the transitions between low-lying states, FFN used the published spectra of the time and assigned spins and parities randomly to states which do not have known spins or parities. For any parent and daughter states which could have allowed transitions, they assigned a  $\log_{10}ft = 5$ . The only exception was in the case of known transitions, where the mea-

sured value was used. For electron capture on  $^{59}\text{Co}$ , the only known transitions which are relevant are the  $^{59}\text{Fe}$   $\beta^-$  decays to  $^{59}\text{Co}$  excited states at 1.482, 1.434, 1.292, and 1.094 MeV, which have  $\log_{10}ft$  values of 7.03, 6.49, 5.98, and 6.70, respectively. Detailed balance is used to compute the electron capture matrix elements.

In our calculations we have superseded the FFN treatment of GT resonances. However, because of the primitiveness of our shell model calculations, we are not able to improve on the FFN treatment of transitions between low-lying states. We thus follow their treatment of these low-lying transitions. The only difference between our rates and the FFN rate is thus the treatment of GT resonances.

The stellar electron capture rates which result from these calculations are shown in Fig. 3. We take the density to be  $10^9 \text{ g cm}^{-3}$ , the density at which  $^{59}\text{Co}$  becomes abundant in a presupernova core. The relevant temperatures are  $T_9 \sim 3-5$ . For temperatures greater than this

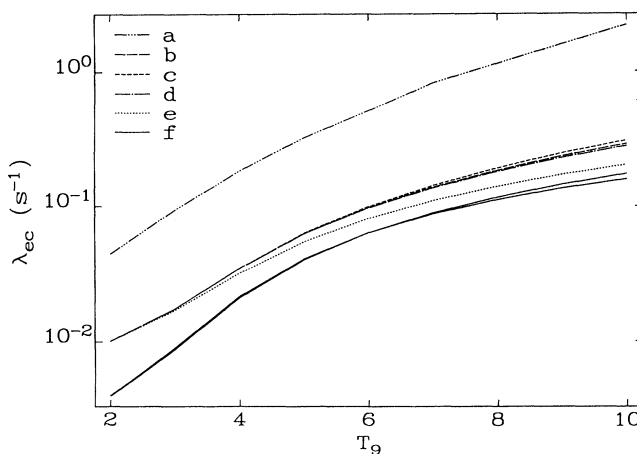


FIG. 3. Electron capture rate on  $^{59}\text{Co}$  versus temperature in units of  $10^9 \text{ K}$ . Curve  $a$  is the FFN rate. Curves  $b$ ,  $c$ , and  $d$  are the rates calculated using strength functions from the small, small modified, and large spaces, respectively. Curves  $e$  and  $f$  are the “optimistic” and “pessimistic” rates, respectively, derived from the experimental data as discussed at the end of Sec. IV.

range, these rates may not be very reliable because high-lying resonances in the parent state have not been included in the rate. These resonances would increase the rate with increasing temperature.  $Y_e$  has been fixed at 0.5, so that comparison with the FFN rates can be made. The small modified model space provides the largest rate because the GT resonance is the lowest in this case, as was seen in Figs. 1 and 2. The small model space yields the next strongest rate, because the GT strength is slightly lower than in the large model space. These differences are trivial compared to the difference between them and the FFN rate. The FFN rate is at least 4.5 times as large because FNN used the ISPSM to estimate the location of the GT strength and thus placed it too low in the daughter. This results in a rate which is much too strong. In the three shell model rates, the GT strength has been placed so high in the daughter that, even at a density of  $10^9 \text{ g cm}^{-3}$ , the electron Fermi energy is not large enough for many electrons to reach the GT resonance.

A comment on the FFN rates is necessary at this point. The original FFN rates [4] did not quench the GT resonances which FNN included. This point is discussed in Sec. IV of the fourth FFN paper [5], where they suggest quenching their rates by some factor, depending on how much of the rate is due to the GT resonances. Comparison of our rate without GT resonances to the FFN rate indicates that, under conditions used in Fig. 3, roughly 90% of the original FFN rate results from GT resonances. The FFN rate plotted in Fig. 3 is thus 55% of the original FFN rate, since we have quenched the GT resonance contribution by a factor of 2, as suggested by Fuller [25]. The FFN rates used in the KEPLER stellar evolution code [26,6] have been quenched in a similar way [25].

Although the  $(n,p)$  experiment has measured  $B_{0j}(\text{GT})_+$ , the 1 MeV resolution of these experiments leads to some ambiguity in how the strength is to be placed. This is particularly true in the third and fourth bins, a region stretching from 1.5 to 3.5 MeV. In each of these bins, not enough states have been identified to be certain where the GT strength lies. There are at least seven states in each bin which could contain the strength. These states are at 1.57 MeV ( $\frac{5}{2}^-$ ), 1.75 MeV ( $\frac{3}{2}^-$  or  $\frac{5}{2}^-$ ) 2.162, 2.278, 2.322, 2.348 MeV ( $\frac{7}{2}^-$ ), 2.390, 2.494, 2.570, 2.947, 3.070, 3.104, 3.160, 3.280, and 3.384 MeV. Spins and parities for each state have been given in parentheses where they are known. The total strength in these bins is  $9.78(-2) \pm 1.17(-2)$  and  $3.29(-1) \pm 1.82(-2)$ , respectively. The strength in the third bin thus could be distributed over the states ranging from 1.57 to 2.494 MeV.

The strength seen in bin 4 could be distinguished over states ranging from 2.57 to 3.384 MeV or even higher, into the next bin. Also, some of the large amount of strength seen in bin 5 could be from states in bin 4. It is thus difficult to place the strength unambiguously for rate calculations.

In order to see the effect of this uncertainty on the electron capture rate, we have computed two rates using only transitions known from the  $\beta^-$  decay of  $^{59}\text{Fe}$  and the  $(n,p)$  data with the ambiguous strength distributed alternatively as high and as low in  $^{59}\text{Fe}$  as is consistent with the  $(n,p)$  measurement. The “optimistic” case (largest possible rate) occurs when the strength is distributed as low as possible in  $^{59}\text{Fe}$ . The strengths at 0.472 and 1.023 MeV are chosen to be the upper ( $1\sigma$ ) limit allowed by the uncertainties:  $B(\text{GT})_{0.472} = 3.66(-2)$  and  $B(\text{GT})_{1.023} = 5.39(-3)$ . All of the strength in the third (fourth) bin is placed in the 1.57 (2.57) MeV state and the upper ( $1\sigma$ ) limit allowed by the uncertainties is again used:  $B(\text{GT})_{1.57(2.57)} = 1.10(-1)$  [3.47(-1)], with all other states in these bins given no strength. The “pessimistic” case (weakest possible rate) places the strength as high in  $^{59}\text{Fe}$  as it could be. The strength at 0.472 (1.023) MeV is chosen to be the lower ( $1\sigma$ ) limit allowed by the uncertainties, i.e.,  $B(\text{GT})_{0.472(1.023)} = 1.58(-3)$  [2.40(-3)]. The lower ( $1\sigma$ ) limit of the strength in bin 3 (4) is placed at 2.494 (3.384) MeV:  $B(\text{GT})_{2.494(3.384)} = 8.61(-2)$  [3.10(-1)]. All other states are given no strength. These cases thus form limits on the actual value of the rate, which will be somewhere between them.

The rates for these two cases are plotted in Fig. 3. The uppermost solid curve corresponds to the lower limit discussed above. These cases are always within a factor of 2.5 of one another, and they can be thought of as defining a window within which the rate due to known transitions will fall. The three shell model rates discussed above used the “optimistic” case for  $B_{0j}(\text{GT})_+$ , known transitions from  $^{59}\text{Fe}$   $\beta^-$  decay, and shell model strength functions for higher-lying parent states. This choice is evidenced by the convergence of the shell model rates to the “optimistic” case at low temperature, where the contribution of excited states is small. Thus the shell model rates are upper limits on the stellar electron capture rate.

The lower solid curve in Fig. 3 shows the rate without the  $(n,p)$  strength function and with no shell model strength functions. At low temperature it joins to the lower limit curve discussed in the previous paragraph. The rates are very close at this temperature because few electrons are able to reach the GT resonance near 4 MeV. But as the temperature increases, the spread of electrons around the Fermi surface becomes much broader, allow-

TABLE V. Dimensions for  $^{60}\text{Co}$  calculations.

$^{60}\text{Co}$		$^{60}\text{Fe}$	
Model space	Dim.	Model space	Dim.
$(1f_{7/2})^{15}(2p_{3/2}, 2p_{1/2}, 1f_{5/2})^5$	708	$(1f_{7/2})^{14}(2p_{3/2}, 2p_{1/2}, 1f_{5/2})^6$	2542
$+(1f_{7/2})^{14}(2p_{3/2}, 2p_{1/2}, 1f_{5/2})^6$	31 130	$+(1f_{7/2})^{13}(2p_{3/2}, 2p_{1/2}, f_{5/2})^7$	72 298

TABLE VI.  $^{60}\text{Co}$  spectrum. All energies are in MeV. The state seen experimentally at 0.543 MeV has no measured spin or parity. A value of  $2^+$  has been assigned to it arbitrarily.

$J^\pi$	Experiment	Small	Small modified
$5^+$	0.000	0.051	0.115
$2^+$	0.059	0.000	0.000
$4^+$	0.277	0.188	0.352
$3^+$	0.288	0.140	0.327
$5^+$	0.436	0.347	0.276
$3^+$	0.506	0.469	0.574
$2^+$	0.543	0.856	0.850
$3^+$	0.614	1.479	1.182
$1^+$	0.739	1.176	1.720
$4^+$	0.786	0.584	1.028

ing a larger proportion to reach the GT resonance. For this reason the rate with the experimental strength function can be distinguished from the rate without it. This effect is the reason why the various rates can be distinguished at high temperature, even though the differences in their resonances are at relatively high daughter excitation energy.

### V. IMPLICATIONS FOR $^{60}\text{Co}$

As was noted above,  $^{60}\text{Co}$  and  $^{59}\text{Co}$  make the largest contribution to neutronization when the density of the stellar plasma approaches  $10^9 \text{ g/cm}^{-3}$ . It is thus relevant to ask what these results imply about  $^{60}\text{Co}$ . In this section we will investigate this question, using the same interactions as were used with  $^{59}\text{Co}$ . This study will tell us whether the strength functions in  $^{60}\text{Co}$  are also higher above the daughter ground state than the ISPSM would have estimated.

We have computed spectra and strength functions for the first 11 states in  $^{60}\text{Co}$ . We have used the small and small modified spaces discussed above. Table V lists the dimensions of the small and large model spaces for the  $^{60}\text{Co}$  system. In view of the small differences between the various rates which used shell model results in the case of  $^{59}\text{Co}$  and the size of the large  $^{60}\text{Co}$  model space, we have chosen only to use the small model space for  $^{59}\text{Co}$ . Table VI compares the experimental and theoretical spectra for

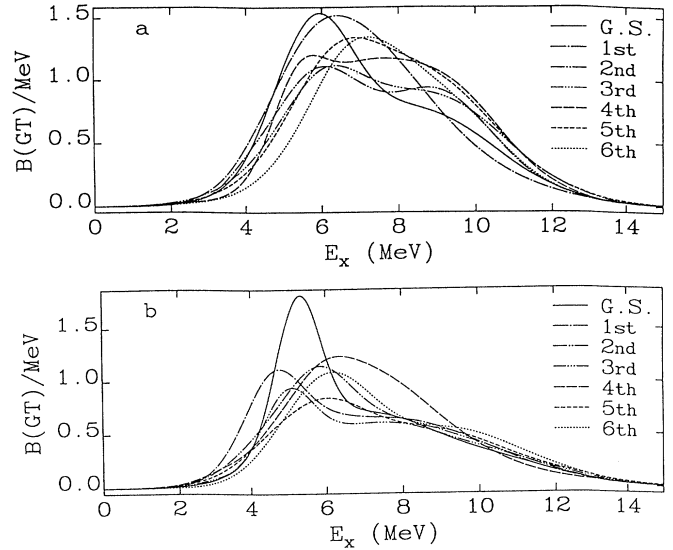


FIG. 4. GT strength functions for the ground state and excited states of  $^{60}\text{Co}$ . The strength functions from the parent states listed in Table VI are listed in the order in which each parent state appears in a particular shell model calculation. The shell model strength functions are given the widths assigned them by the Lanczos process after ten iterations for each allowed daughter  $J^\pi$ , added in quadrature with the experimental resolution of 1 MeV (full width at half maximum). None of the strength functions have been quenched. (a) and (b) correspond to the small and small modified model spaces, respectively.

$^{60}\text{Co}$ . As was the case for  $^{59}\text{Co}$ , the modified case provides slightly poorer agreement with experimental spectra than the original interaction.

In Fig. 4 the strength functions corresponding to the lowest seven theoretical states of  $^{60}\text{Co}$  are given. Table VII lists the total strength and centroids of those strength functions. It can be seen that the Brink assumption is qualitatively satisfied, but more poorly than in the case of  $^{59}\text{Co}$ . Now the centroids follow the parent state excitation energies to within only 300 keV. This poorer agreement may be due to the more complicated low energy structure of  $^{60}\text{Co}$ . The FFN approach would have placed the centroid of the ground state strength function 3.55 MeV above the daughter ground state.

TABLE VII. GT strengths and centroids for  $^{60}\text{Co}$ . All energies are given in MeV. The centroid of a given strength function is  $\bar{E}$ .  $\bar{E}_0$  is the centroid of the strength function from the ground state of  $^{60}\text{Co}$  nucleus.

$E_i$	Small space		$E_i$	Small modified space	
	$\bar{E} - \bar{E}_0$	$B(\text{GT})$		$\bar{E} - \bar{E}_0$	$B(\text{GT})$
0.000	0.000	0.67	0.000	0.000	7.09
0.051	-0.004	5.66	0.115	-0.110	7.54
0.140	0.221	5.66	0.276	0.309	6.66
0.188	0.437	4.77	0.327	0.476	6.75
0.347	0.252	6.26	0.352	0.507	7.45
0.469	0.596	5.03	0.574	0.563	7.56
0.584	0.712	5.49	0.850	0.676	6.66

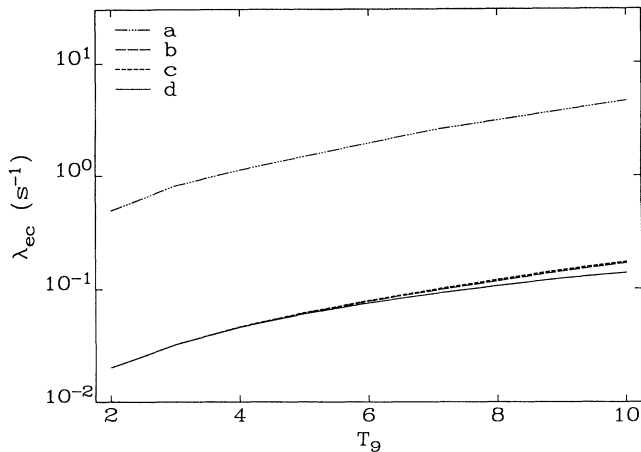


FIG. 5. Electron capture rate on  $^{60}\text{Co}$  versus temperature in units of  $10^9$  K. Curve *a* is the FFN rate. Curves *b* and *c* are the rates calculated using strength functions from the small and small modified spaces, respectively. Curve *d* is the rate without any GT resonance strength.

These strength functions have been quenched by the same amount as in the case of  $^{59}\text{Co}$  and combined into stellar rates. We have also computed a rate which has no GT resonances in it. Figure 5 compares the rates with the results of Fuller, Fowler, and Newman. There is little difference between the various rates which we have computed. All three rates computed here are more than a factor of 10 less than the FFN rate. This is again a result of the placement of the GT strength. The experimental results force us to place the GT resonance at least 5 MeV above the daughter ground state, much higher than the FFN estimate would have placed it. As a result, at these densities very few electrons are able to make captures to the resonance, despite its enhanced matrix element. This fact can be seen in the very small differences between the rates with and without GT resonances included. The FFN rate placed the resonance much lower in the daughter nucleus, thus allowing a very large number of electrons to make the very strong transition.

As was the case for  $^{59}\text{Co}$ , the FFN rate plotted in Fig. 5 has been quenched. For these conditions, only 2% of the original FFN rate comes from nonresonant contributions. Thus the rate plotted is 51% of the original FFN rate, again quenching the GT strength by a factor of 2.

In the previous sections, we have used the results from the charge-exchange experiment on  $^{59}\text{Co}$  to calibrate our shell model calculations. We have assumed that this calibration is valid for  $^{60}\text{Co}$ . This assumption will be tested in a future paper [21], but it can be seen in Fig. 5 that the exact placement of the GT resonance does not have a large effect on the rate because it is so high.

## VI. CONCLUSIONS

The recent  $^{59}\text{Co}(n,p)^{59}\text{Fe}$  experiment shows a GT resonance at 4 MeV, much higher above the  $^{59}\text{Fe}$  ground state than one would expect based upon a simple indepen-

dent single particle shell model extrapolation of data from the  $^{54}\text{Fe}(n,p)^{54}\text{Mn}$  reaction. The height of this resonance seems to be a result of the interaction between the additional neutrons in  $^{59}\text{Co}$ , which push the resonance higher in energy. This behavior is seen qualitatively in shell model calculations which include configuration mixing.

The GT resonances from more highly excited states cannot be measured at present. We are thus forced to rely on the shell model calculations. These resonances, as calculated by the full shell model, adequately satisfy the Brink assumption and are thus also very high above the  $^{59}\text{Fe}$  ground state. As a result, the stellar electron capture rate for  $^{59}\text{Co}$  is much smaller than previously has been predicted.

It has also been found that the GT strength in  $^{60}\text{Co}$  is pushed fairly high above the daughter ground state because of configuration mixing. This effect results in  $^{60}\text{Co}$  also having a much weaker electron capture rate than previous work had indicated. It appears likely that this behavior is a general feature of nuclei in this region. Thus it is our expectation that similar reductions in rates will be seen for all nuclei near  $^{59}\text{Co}$ , because they too will experience the configuration mixing effects which weaken and push the GT strength to higher excitation energies in the daughter.

These weaker rates can have an effect on the evolution of presupernova models. A reduction of rates, as envisaged here, will decrease the neutronization of the forming iron core. Because the mass of the iron core goes roughly as  $Y_e^2$ , a reduction of electron capture rates in the model will lead to a larger iron core. A larger core is more difficult to explode after core collapse because of the larger amount of material which the shock must photodissociate before it can pass [27–29]. However, a larger value of  $Y_e$  will also lead to shock formation farther out in the iron core [27,28]. It is not possible to make accurate predictions of the consequences of these rates at present.

What is needed are shell model calculations which more reliably predict the location of GT strength in unstable nuclei which are difficult to measure, but are important in presupernova cores. We are currently seeking ways to improve the reliability of shell model calculations in predicting GT strength and other nuclear parameters relevant to determining stellar electron capture rates. Better knowledge of the actual effect on presupernova evolution will come from these new rates when they have been used in evolution calculations. Whatever the final answers will be, the results of the  $(n,p)$  experiments studied here will mandate a reevaluation of stellar electron capture rates.

## ACKNOWLEDGMENTS

We thank the CHARGEX group at TRIUMF for making its data available before formal publication and Dr. W. P. Alford for useful discussions on how to interpret these experiments. We thank Dr. G. E. Brown for

suggesting this study. We thank the Institute for Nuclear Theory at the University of Washington for hosting the workshop “Nuclear Astrophysics of Type II Supernovae: The Fifth Anniversary of SN1987A,” during which much

of this paper was prepared. Work at LLNL was performed under the auspices of the U.S. Department of Energy under Contract No. W-7405-ENG-48 and DOE Nuclear Theory Grant No. SF-ENG-48.

- 
- [1] H. A. Bethe, G. E. Brown, J. Applegate, and J. Lattimer, *Nucl. Phys.* **A234**, 487 (1979).
  - [2] G. M. Fuller, W. A. Fowler, and M. J. Newman, *Astrophys. J. Suppl.* **42**, 447 (1980).
  - [3] G. M. Fuller, W. A. Fowler, and M. J. Newman, *Astrophys. J.* **252**, 715 (1982).
  - [4] G. M. Fuller, W. A. Fowler, and M. J. Newman, *Astrophys. J. Suppl.* **48**, 279 (1982).
  - [5] G. M. Fuller, W. A. Fowler, and M. J. Newman, *Astrophys. J.* **293**, 1 (1985).
  - [6] T. A. Weaver, S. E. Woosley, and G. M. Fuller, in *Numerical Astrophysics*, edited by J. M. Centrella, J. M. LeBlanc, and R. L. Bowers (Jones & Bartlett, Boston, 1985), p. 374.
  - [7] A. García *et al.*, *Phys. Rev. Lett.* **67**, 3654 (1991).
  - [8] J. Rapaport *et al.*, *Phys. Rev. Lett.* **47**, 1518 (1981).
  - [9] M. B. Aufderheide, S. D. Bloom, D. A. Resler, and C. D. Goodman, *Phys. Rev. C* **40**, 2251 (1993).
  - [10] D. P. Wells, *Bull. Am. Phys. Soc.* **37**, 1296 (1992).
  - [11] G. M. Fuller and B. S. Meyer, *Astrophys. J.* **376**, 701 (1991).
  - [12] M. B. Aufderheide, *Nucl. Phys.* **A526**, 161 (1991).
  - [13] M. C. Vetterli *et al.*, *Phys. Rev. C* **40**, 559 (1989).
  - [14] W. P. Alford *et al.*, *Bull. Am. Phys. Soc.* **37**, 1298 (1992).
  - [15] W. P. Alford *et al.*, submitted to *Phys. Rev. C*.
  - [16] C. Gaarde *et al.*, *Nucl. Phys.* **A334**, 248 (1980).
  - [17] B. A. Brown and B. H. Wildenthal, *At. Data Nucl. Data Tables* **33**, 347 (1985).
  - [18] P. Bopp *et al.*, *Phys. Rev. Lett.* **56**, 919 (1986).
  - [19] A. van Hees and P. Glaudemans, *Z. Phys. A* **303**, 267 (1981).
  - [20] J. van Hienen, W. Chung, and B. H. Wildenthal, *Z. Phys. A* **269**, 159 (1976).
  - [21] M. B. Aufderheide, S. D. Bloom, D. A. Resler, and G. J. Mathews, submitted to *Phys. Rev. C*.
  - [22] D. A. Resler and S. M. Grimes, *Comput. Phys.* **2**, 65 (1988).
  - [23] D. M. Brink, *Rep. Prog. Phys.* **21**, 144 (1958).
  - [24] C. D. Goodman and S. D. Bloom, in *Spin Excitations in Nuclei*, edited by F. Petrovich *et al.* (Plenum, New York, 1982), p. 143.
  - [25] G. M. Fuller (private communication).
  - [26] T. A. Weaver, G. B. Zimmerman, and S. E. Woosley, *Astrophys. J.* **225**, 1021 (1978).
  - [27] A. Burrows and J. Lattimer, *Astrophys. J.* **270**, 735 (1983).
  - [28] J. Cooperstein, H. A. Bethe, and G. E. Brown, *Nucl. Phys.* **A429**, 527 (1984).
  - [29] E. A. Baron, Ph.D. thesis, SUNY at Stony Brook, 1985.